

Article

Elucidation of Structures, Electronic Properties, and Chemical Bonding of Monophosphorus-Substituted Boron Clusters in Neutral, Negative, and Positively Charged $PB_n/PB_n^-/PB_n^+$ ($n = 4-8$)

Qing-Shan Li ^{1,2,3,†}, Bingyi Song ^{1,2,3,†}, Limei Wen ^{1,2,3}, Li-Ming Yang ^{1,2,3,*} and Eric Ganz ⁴ 

¹ Key Laboratory of Material Chemistry for Energy Conversion and Storage, Ministry of Education, School of Chemistry and Chemical Engineering, Huazhong University of Science and Technology, Wuhan 430074, China

² Hubei Key Laboratory of Bioinorganic Chemistry and Materia Medica, School of Chemistry and Chemical Engineering, Huazhong University of Science and Technology, Wuhan 430074, China

³ Hubei Key Laboratory of Materials Chemistry and Service Failure, School of Chemistry and Chemical Engineering, Huazhong University of Science and Technology, Wuhan 430074, China

⁴ School of Physics and Astronomy, University of Minnesota, 116 Church St. SE, Minneapolis, MN 55455, USA

* Correspondence: lmyang@hust.edu.cn

† These authors contributed equally to the work and are co-first authors.

Abstract: This paper reports the computational study of phosphorus-doped boron clusters $PB_n/PB_n^-/PB_n^+$ ($n = 4-8$). First, a global search and optimization of these clusters were performed to determine the stable structures. We used density functional theory (DFT) methods and ab initio calculations to study the stability of the atomic clusters and to explore the arrangement of stable structures. We found that the lowest energy structures of the smaller phosphorus-doped boron clusters tend to form planar or quasi-planar structures. As additional boron atoms are added to the smallest structures, the boron atoms expand in a zigzag arrangement or in a net-like manner, and the phosphorus atom is arranged on the periphery. For larger structures with seven or eight boron atoms, an unusual umbrella-like structure appears. We calculated the binding energy as well as other energies to study cluster stability. We calculated the ionization energy, electron affinity, and the HOMO–LUMO gaps. In addition, we used the adaptive natural density partitioning program to perform bond analysis so that we have a comprehensive understanding of the bonding. In order to have a suitable connection with the experiment, we simulated the infrared and photoelectron spectra.

Keywords: phosphorus-doped boron clusters; hypercoordinate; AdNDP; density functional theory; DFT; ab initio calculations; infrared spectrum; photoelectron spectrum



Citation: Li, Q.-S.; Song, B.; Wen, L.; Yang, L.-M.; Ganz, E. Elucidation of Structures, Electronic Properties, and Chemical Bonding of Monophosphorus-Substituted Boron Clusters in Neutral, Negative, and Positively Charged $PB_n/PB_n^-/PB_n^+$ ($n = 4-8$). *Condens. Matter* **2022**, *7*, 66. <https://doi.org/10.3390/condmat7040066>

Academic Editor: Bohayra Mortazavi

Received: 15 September 2022

Accepted: 9 November 2022

Published: 12 November 2022

Publisher's Note: MDPI stays neutral with regard to jurisdictional claims in published maps and institutional affiliations.



Copyright: © 2022 by the authors. Licensee MDPI, Basel, Switzerland. This article is an open access article distributed under the terms and conditions of the Creative Commons Attribution (CC BY) license (<https://creativecommons.org/licenses/by/4.0/>).

1. Introduction

The exploration of boron clusters has developed rapidly over the past few decades due to boron being a typical electron-deficient atom. When clusters are formed, many strong multi-center chemical bonds can be formed. Therefore, related research on boron clusters has been widely pursued. The stable structures of gas-phase anion clusters B_n^- ($n = 3-25, 27-30, 35, 36$) [1–10] of pure boron clusters have been experimentally verified. Due to the superior physicochemical properties of experimentally observed pure boron clusters, the study of doped boron clusters has been a hot topic [11]. Related studies have shown that some boron clusters have unique aromaticity and the ability to store hydrogen [12,13]. For example, one can consider the related physicochemical properties of aluminum-doped boron clusters and what kind of arrangement characteristics are formed when forming stable structures. In the field of aluminum-doped boron clusters, there is a relatively mature understanding. Experimental studies have shown that boron clusters can be used as raw materials for the preparation of metal nanocomposites, and boron clusters play an important role as reducing agents and stabilizers in the preparation process [14]. It

has also been reported that non-metal/heavy atom boron clusters can be used to prepare high-performance phosphors [15]. In recent years, there has been outstanding research progress in terms of the electronic stability, bonding properties, and chemical reactivity of closo- $[\text{B}_n\text{X}_n]^{2-}$ dianions as a function of boron cage scaffold n ($n = 12, 11, 10, 6$) as well as the ligand X ($X = \text{H}, \text{F}, \text{Cl}, \text{Br}, \text{I}, \text{CN}$) [16–20]. However, there are few theoretical studies on the doping of boron clusters with phosphorus atoms. There is only a small amount of carbon and phosphorus doping-related research [21].

We recently published a paper on similar P_2B_n systems [22]. Other pertinent work includes doped small boron clusters [23] and aluminum-doped boron clusters [24]. A number of other related interesting results have been recently published [25–32]. In order to have a comprehensive understanding of the global structure and properties of phosphorus-doped boron clusters, we systematically studied the mono-phosphorus-doped boron clusters.

2. Computational Methods

We first performed a global search for the stable structure of $\text{PB}_n/\text{PB}_n^-/\text{PB}_n^+$ clusters. The traditional method is minima hopping (MH) search [33–35]. This is carried out through molecular dynamics and local optimization only on the potential energy surface. This can waste computing resources by repeatedly searching for structures on the same potential energy surface. An alternative method uses basin-hopping [36]. This has certain advantages compared with the previous MH method but is still not perfect. That is, if there is an invalid disturbance in the global search, or the structure obtained after the disturbance does not conform to the normal arrangement, then a repeated search cannot be avoided. These disturbances appear because the change of energy is a single variable. We used the Coalescence Kick (CK) [37] program written by Averkiev, which is superior to the previous two methods. The initial structure of the cluster $\text{PB}_n/\text{PB}_n^-/\text{PB}_n^+$ was generated by this program, followed by preliminary optimization of the structure. Due to the roughness of the initial structure, it is not advisable to use a higher precision method and basis set. Therefore, we started with HF/STO – 3G [38] to optimize the initial structure. These structures still required further optimization. Next, we used the B3LYP/6 – 31G (d) [39,40] method and basis set for all optimization and frequency calculations. The lowest energy structures were now located. Single point energies at the accurate CCSD (T)/6 – 311 + G (2df) level were calculated. The relative energies using B3LYP/6 – 311 + G (d) were also calculated as a comparison.

To determine the stability of these structures, we calculated the binding energies and different energies. Next, we calculated the ionization energies and electron affinities of the clusters. We then determined the HOMO–LUMO gap [41,42] values. Finally, an adaptive natural density partitioning program (AdNDP) analysis was performed. In order to make a connection between theoretical research and experiment, we carried out the calculation of the infrared spectrum and photoelectron spectroscopy. This paper is part of a series of papers on PB_n clusters. For consistency, we maintained the same computational methods for the entire series.

3. Results and Discussion

3.1. Growth Behavior of Different Sized Phosphorus-Doped Boron Clusters

3.1.1. Structure of Neutral PB_n ($n = 4–8$) Clusters

The point groups, electronic states, relative energies, and structures of the neutral clusters PB_n are listed in Figure 1. Considering the isomers of PB_4 , we observe that the four boron atoms are arranged in a parallelogram, and the phosphorus atom is arranged around the flat quadrilateral. When the parallelogram formed by the boron atoms is broken, the energy increases. For example, it can be seen by a comparison of the $4n-1$ structure with the $4n-2$ structure. The relative energy of $4n-2$ is 38.13 kcal/mol, which is much larger than $4n-1$, indicating that $4n-1$ is the global minimum and the most stable structure of cluster PB_4 .

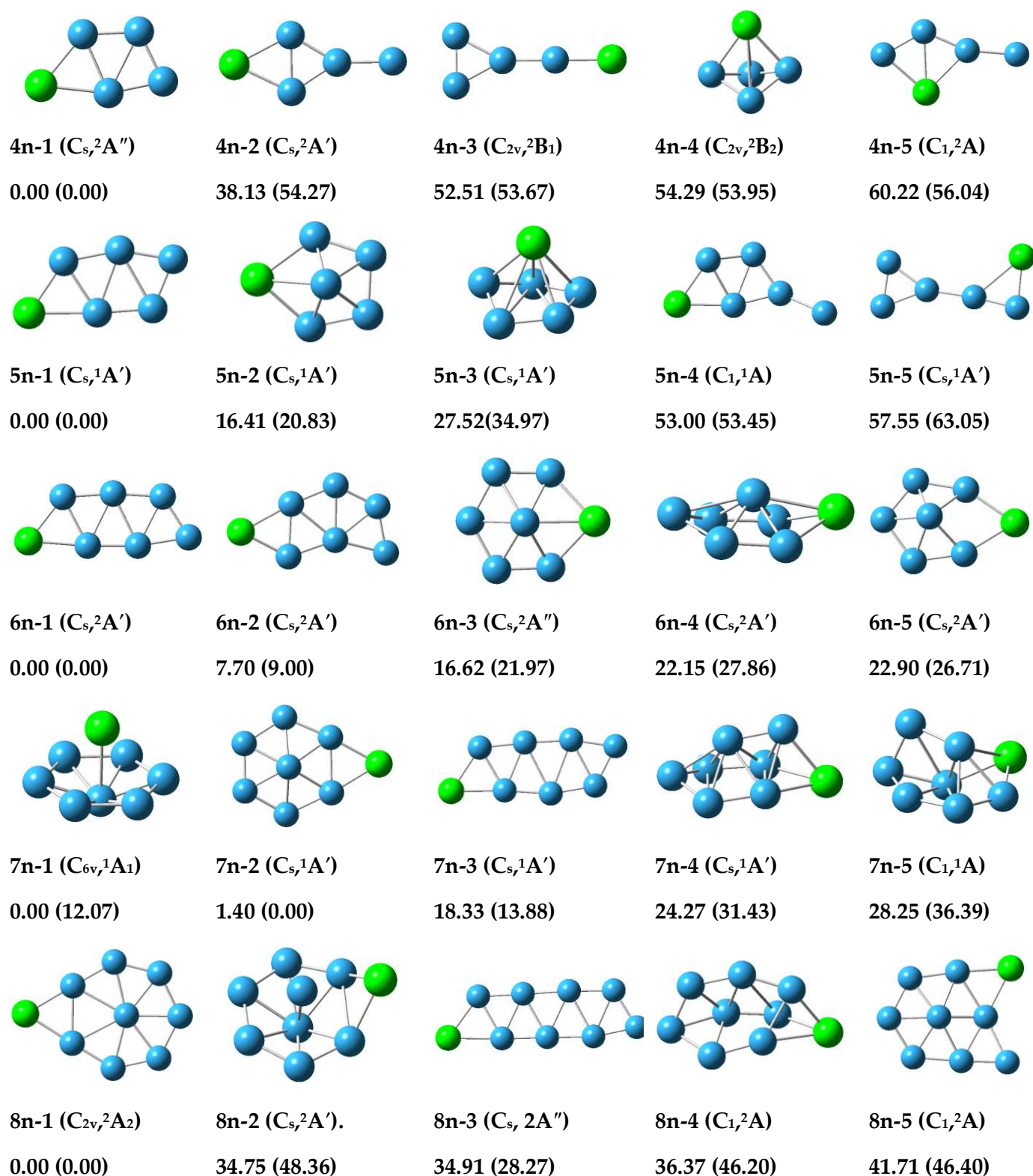


Figure 1. The optimized geometries of neutral PB_n clusters. The relative energies in kcal/mol are listed under each structure using CCSD (T)/6 – 311 + G (2df). The relative energies using B3LYP/6 – 311 + G (d) are in parentheses.

For the neutral PB_5 cluster, the five B atoms of the lowest energy structure 5n-1 form a triangular 2D raft. The P atom is located in the outer position. Comparing the structures of 4n-1 and 5n-1, it can be seen that B atoms grow in a zigzag pattern. Therefore, the presence

of P atoms does not change the preference of the B atoms to form triangular 2D rafts. The relative energy of 5n-2 is 16.41 kcal/mol, and the 5n-1 structure is the global minimum and the most stable structure of cluster PB_5 .

For the neutral PB_6 cluster, the 6n-1 structure is similar to that of 5n-1. The B atoms are arranged in a narrow 2D zigzag pattern based on triangular elements. The P atom is located on the periphery. The 6n-2, 6n-3, and 6n-5 structures can be seen as mesh structures, which are formed by adding a boron atom onto different locations of the 5n-2 structure. 6n-2 and other structures have higher relative energies, indicating that 6n-1 is the global minimum and the most stable structure of cluster PB_6 . From the perspective of relative energy, for the six boron structures, the zigzag structure is lower energy than the mesh structure.

In Figure 1, the most stable structure of the neutral cluster PB_7 is significantly different from the first three clusters of PB_6 . When the number of boron atoms is increased to seven, the boron atoms and the phosphorus atoms are arranged in an unusual and appealing umbrella shape. This has C_{6v} symmetry. The seven boron atoms form a concave hexagon, and the single phosphorus atom is located directly above the concave hexagon. It has the highest stability using CCSD (T) but not with B3LYP. The 7n-2 structure forms a mesh structure, like 6n-3 and 6n-5. The relative energy of the 7n-3 structure arranged in a zigzag shape is significantly greater than that of the 7n-2 structure. When the number of boron atoms is increased to seven, the umbrella structure or mesh structure is better than the zigzag structure.

For the neutral PB_8 cluster, the most stable 8n-1 structure is a mesh structure rather than a zigzag structure. The center of the structure is a boron atom, and it is surrounded by a heptagonal structure of seven boron atoms. This could be considered a molecular wheel. The phosphorus atom is arranged on the periphery, and their shape forms a planar structure with C_{2v} symmetry and 2A_2 electronic state. In contrast, the structure 8n-3 formed in a zigzag arrangement has a higher relative energy. Similar to the PB_7 clusters, the network structure is better than the zigzag structure.

3.1.2. Structure of Anionic PB_n^- Clusters

The structures, symmetries, electronic states, and relative energies of anionic PB_n^- clusters are shown in Figure 2. For the anionic PB_4^- cluster, the 4a-1 structure with the P atom at the periphery of the boron quadrilateral is similar to the 4n-1 structure, which is the global minimum of the cluster. For the PB_5^- and PB_6^- clusters, the 5a-1 and 6a-1 structures can be seen as growing via an extension of the zigzag on the 4a-1 structure. The structures of 5a-1 and 6a-1 are the global minima and the most stable structures of PB_5^- and PB_6^- clusters. The structures 5a-2 and 6a-2 are net-like, and the relative energies are 12.42 and 20.46 kcal/mol higher than the global minimum, respectively. Therefore, when $n \leq 6$, the zigzag structure is more stable than the mesh structure. This conclusion is the same as that of neutral clusters.

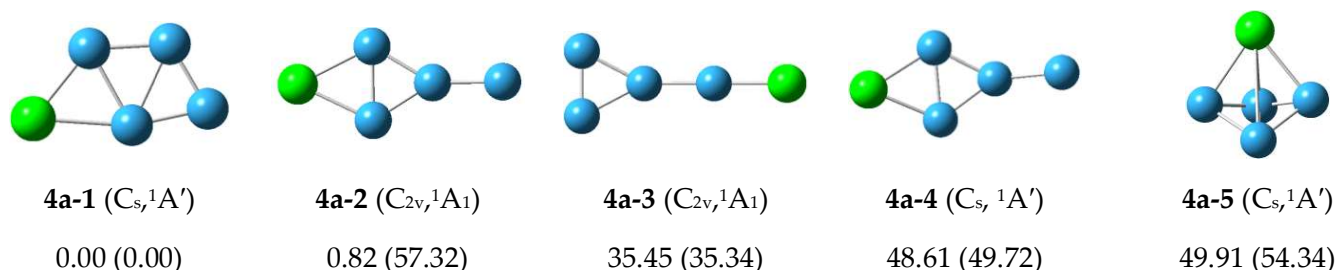


Figure 2. Cont.

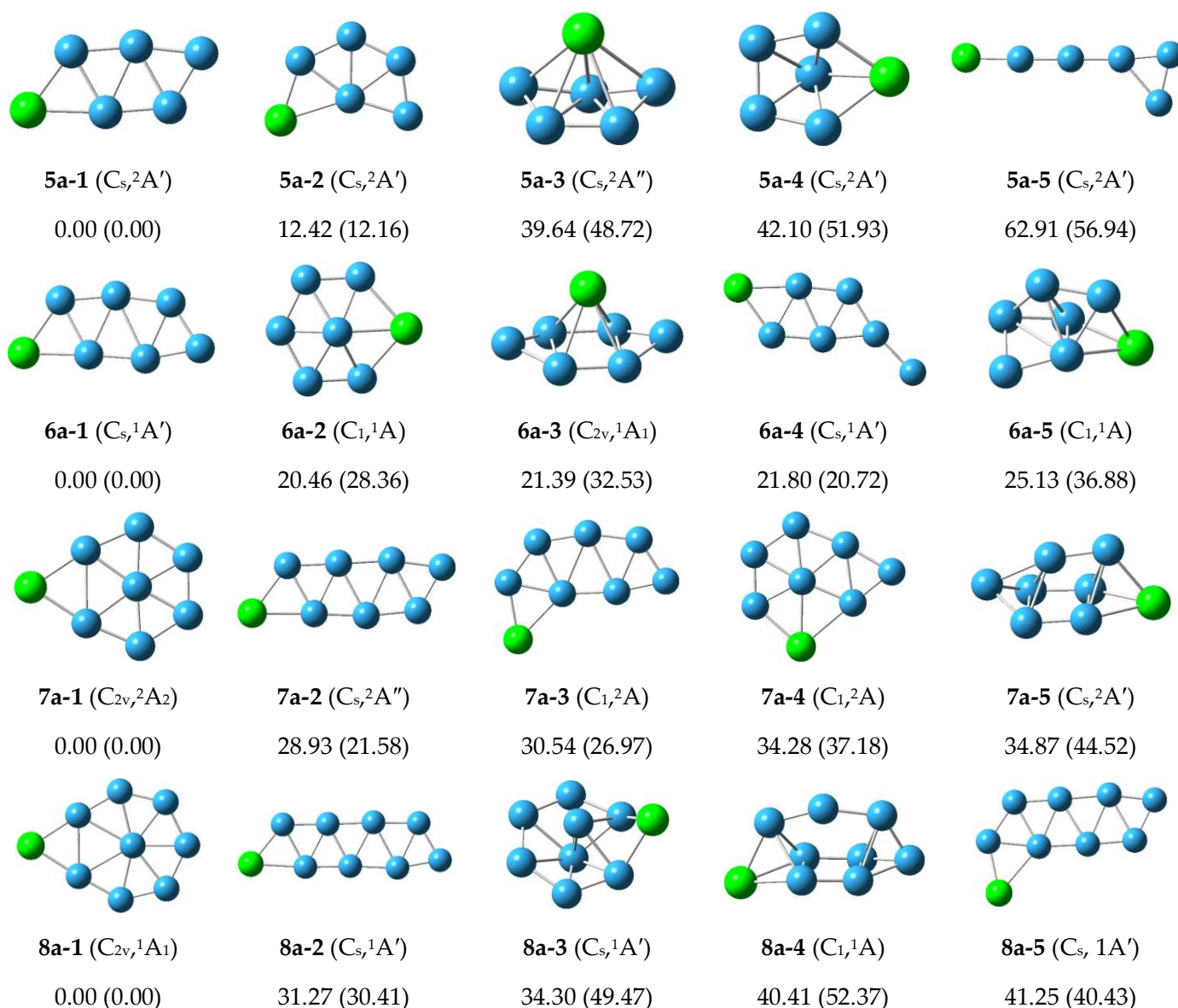


Figure 2. The optimized geometries of anionic PB_n^- clusters. The relative energies (kcal/mol) were based on CCSD(T)/6-311+G(2df) calculations. B3LYP energies are in parentheses.

When $n = 7$, for the PB_7^- cluster, the neutral $7n-1$ structure is an umbrella structure, while the anionic $7a-1$ structure has a planar structure with C_{2v} symmetry and 2A_2 electronic state. The $7a-1$ structure is the global minimum, which is similar to the $7n-2$ structure. The net-like structure of $7a-1$ is more stable than the zigzag structure of $7a-2$. When $n = 8$, for the PB_8^- cluster, the $8a-1$ structure is the same as the $8n-1$ structure, which is the global minimum and the most stable structure of the cluster. The $8a-2$ structure has relative energy of 31.27 kcal/mol and grows in a zigzag shape. The $8a-1$ mesh structure is more stable than the $8a-2$ zigzag structure.

The structures, symmetries, electronic states, and relative energies of cationic PB_n^+ clusters are shown in Figure 3. For the cationic PB_4^+ cluster, the planar structure of $4c-1$ with C_s symmetry is similar to the $4n-1$ and $4a-1$ structure, which is the global minimum of the PB_4^+ cluster. For the cationic PB_5^+ cluster, the structure of $5c-1$ is similar to the structures of $5a-1$ and $5n-1$, with their internal boron atoms still growing linearly in a zigzag pattern. Phosphorus atoms are arranged at the outermost periphery of the structure. The structure of $5c-2$ is similar to the structure of $5n-2$, which is 20.50 kcal/mol higher energy

than 5c-1. It is worth noting that one boron atom at the edge of each of the structures 5c-4 and 5c-5 are arranged with a single bond, which causes a significant increase in energy.

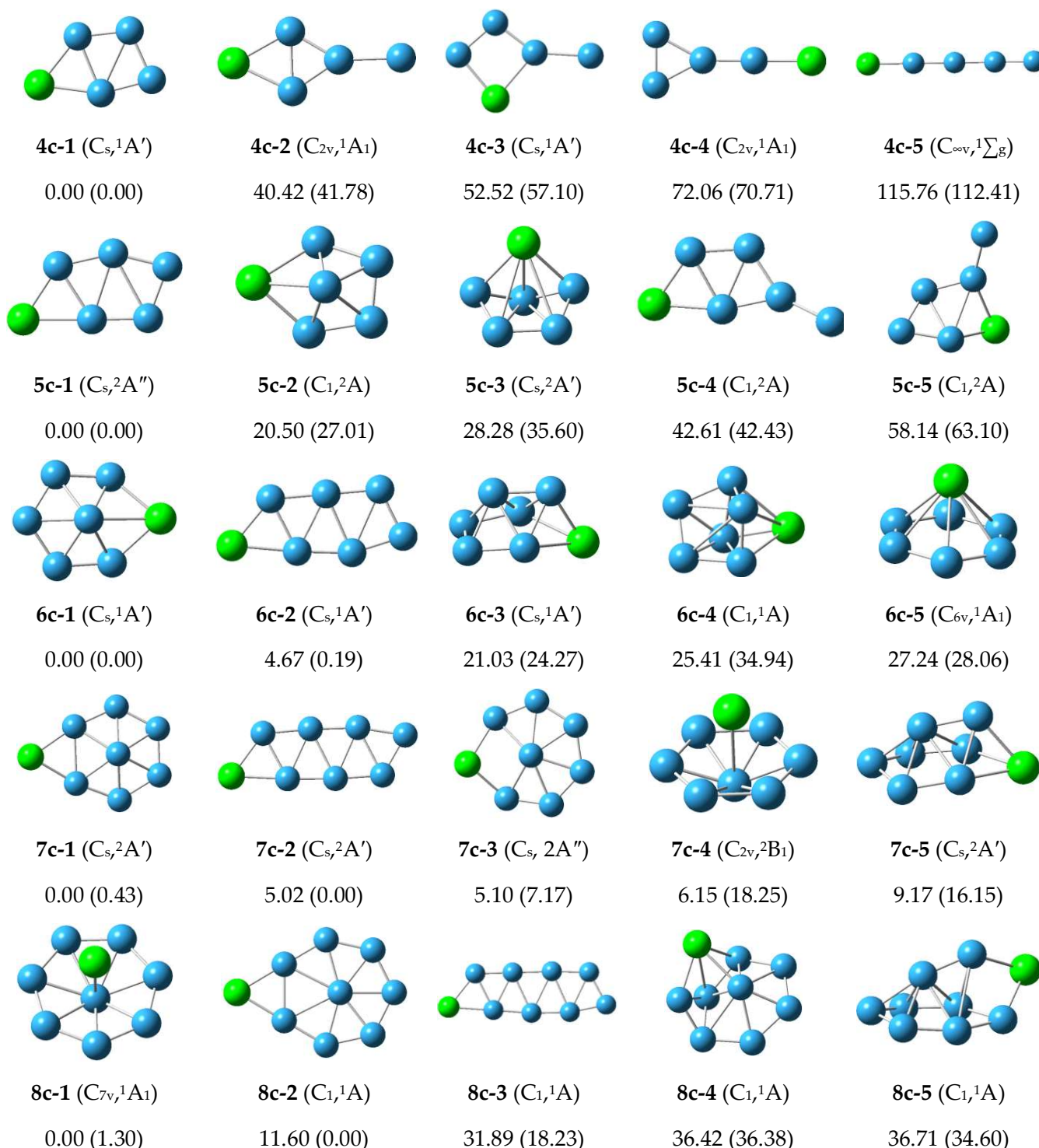


Figure 3. The optimized geometries of cationic PB_n^+ clusters. The relative energies (kcal/mol) from CCSD (T)/6-311+G (2df). The B3LYP energies are in parentheses.

For the cationic PB_6^+ cluster, the 6c-1 structure can be seen as net-like addition to the 4c-1 and 5c-2 structures. The 6c-1 structure is the global minimum and the most stable structure of the PB_6^+ cluster. The 6c-2 structure is in a zigzag shape, and the relative energy is 4.67 kcal/mol higher than the global minimum 6c-1, indicating that when $n \geq 6$, the

network structure is more stable than the zigzag structure. This conclusion is somewhat different from the neutral and anionic clusters. When the 6c-1 structure and the 6c-2 structure in Figure 3 are arranged in an anionic structure, and a neutral molecular structure, the stability of the former is lower than that of the latter. With a positive charge, the stability changes. The reason may be that the hexagonal structure of 6c-1 is close to the planar structure. The phosphorus atom is an electron-rich atom with a lone pair of electrons. For this reason, the stability of 6c-1 is slightly higher than that of the 6c-2 structure.

When $n = 7$, for the cationic PB_7^+ cluster, the 7c-1 structure is the global minimum, which is similar to the 7n-2 and 7a-1 structure and has higher stability, which may be due to its planar ring structure. When a six-membered ring structure composed of boron atoms carries a unit of positive charge, the lone pair of electrons of the phosphorus atom can delocalize to the hexagonal structure formed by the boron atom, and neutralizing a portion of the positive charge enhances the stability of the entire structure. In addition, it can be seen from the figure that the 7c-1 mesh structure has lower energy than the zigzag structure of 7a-2 and the umbrella structure 7c-4, so the 7c-1 structure is better than 7a-2 and 7c-4.

The structure of 8c-1 in Figure 3 is unusual because the boron atom in the 8c-1 structure forms an umbrella-like structure. The reason why the structure has high stability may be that seven boron atoms form a large planar structure. When a positive charge is applied to this structure, it is beneficially distributed by the unique position of the phosphorus atom. The structures 8c-2 to 8c-5 show different possibilities.

It is interesting to compare the results of this paper on PB_n to our previous work on P_2B_n clusters [22]. For PB_n for larger structures with 7 or 8 boron atoms, an unusual umbrella-like structure appears. This structure is rarely seen. This is not seen in the lowest energy P_2B_n structures. The HOMO–LUMO gaps are much larger for P_2B_n than PB_n .

3.2. Relative Stabilities

In Table 1, E_b represents the average cohesive energy of the phosphorus–boron clusters, and Δ_1E is the fragmentation energy. This is calculated by comparing the energy of a cluster with one less boron plus the energy of the boron atom alone with the cluster energy. Larger values correspond with more stability. Δ_2E is the energy difference of the two clusters with one additional and one fewer B atom minus twice the energy of the original cluster. Δ_2E is also related to cluster stability under growth or annealing conditions.

Table 1. Calculation formula for atomic cluster stability measurement.

PB_n	$E_b(PB_n) = [E(P) + nE(B) - E(PB_n)]/(1+n)$	(1)
	$\Delta_1E(PB_n) = E(PB_{n-1}) + E(B) - E(PB_n)$	(2)
	$\Delta_2E(PB_n) = E(PB_{n-1}) + E(PB_{n+1}) - 2E(PB_n)$	(3)
PB_n^-	$E_b(PB_n^-) = [E(P^-) + nE(B) - E(PB_n^-)]/(1+n)$	(4)
	$\Delta_1E(PB_n^-) = E(PB_{n-1}^-) + E(B) - E(PB_n^-)$	(5)
	$\Delta_2E(PB_n^-) = E(PB_{n-1}^-) + E(PB_{n+1}^-) - 2E(PB_n^-)$	(6)
PB_n^+	$E_b(PB_n^+) = [E(P) + (n-1)E(B) + E(B^+) - E(PB_n^+)]/(1+n)$	(7)
	$\Delta_1E(PB_n^+) = E(PB_{n-1}^+) + E(B) - E(PB_n^+)$	(8)
	$\Delta_2E(PB_n^+) = E(PB_{n-1}^+) + E(PB_{n+1}^+) - 2E(PB_n^+)$	(9)

In Figure 4a, we see that the average cohesive energies are gradually increasing as the number of atoms increases. Therefore, the clusters with more atoms are more stable. The anions are slightly more stable than the others. The values range from 3.7 to 4.7 eV. Considering the fragmentation energy, in Figure 4b, we see that for anionic clusters, $n = 6$ has a lower Δ_1E . For neutral and cationic clusters, we see that $n = 8$ has higher values. In Figure 4c, for the anionic clusters, for $n = 5$, the Δ_2E value is higher; when $n = 6$, it is lower. For anion $n = 6$, this suggests lower stability during growth conditions. For neutral and cationic clusters, $n = 7$ has lower values.

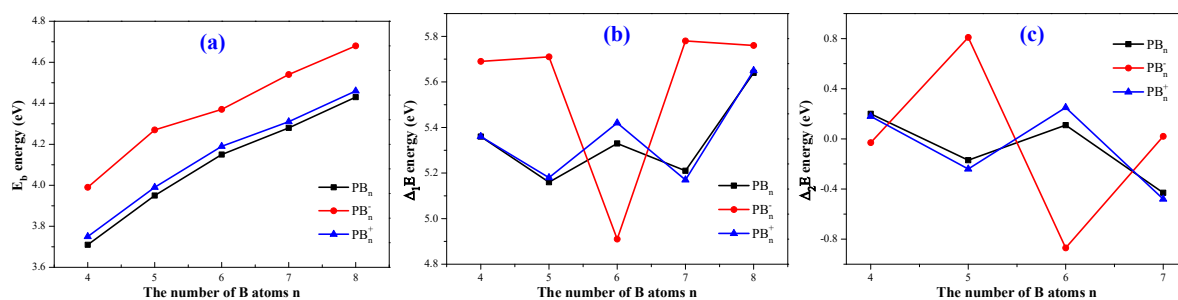


Figure 4. (a–c) show E_b , Δ_1E , and Δ_2E , respectively.

3.3. HOMO–LUMO Gaps

To better understand the properties of the $PB_n/PB_n^-/PB_n^+$ systems, we calculated the HOMO–LUMO gaps in each system. It can be seen from Figure 5 that the HOMO–LUMO gaps are all large. For $n = 4$ and $n = 5$, the gaps range between 2 and 3 eV. For $n = 6$, The cation gap is substantially larger, while the anion is lower. For $n = 7$, the neutral gap is substantially larger than the others. For $n = 8$, the cation gap is twice as large as the other two and the largest in the study.

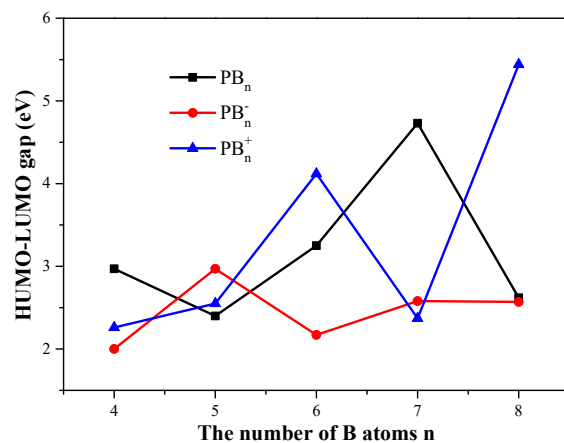


Figure 5. HOMO–LUMO gaps of $PB_n/PB_n^-/PB_n^+$.

3.4. The Ionization Potential (IP) and Electron Affinity (EA)

Figure 6 shows the ionization energies and electron affinity energies of these systems. We can see that the ionization energy (IP) stays roughly constant, near 8.3 eV. The electron affinity (EA) is increasing slowly for these systems from roughly 2.2 to 3 eV.

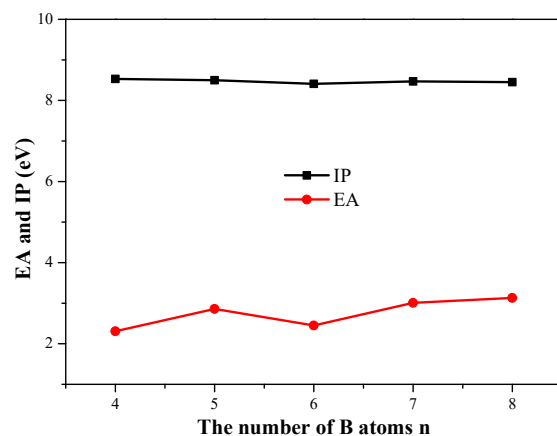


Figure 6. Ionization potential and electron affinity of PB_n clusters.

3.5. Chemical Bonding Analysis

Figure 7 shows the chemical bonding analysis for the neutral 4n-1 structure. The structure has nine bonds in total. This consists of four 2c-2e chemical bonds, one P-B σ bond (with ON = 1.99), and three B-B σ bonds (the ON value range from 1.93 to 1.98). Then there are two 3c-2e σ bonds with an ON value between 1.96 and 1.99. The π bonds of the next two 3c-2e have ON = 1.99 and 1.91, respectively. The last bond is a 4c-2e σ bond, with ON = 1.95.

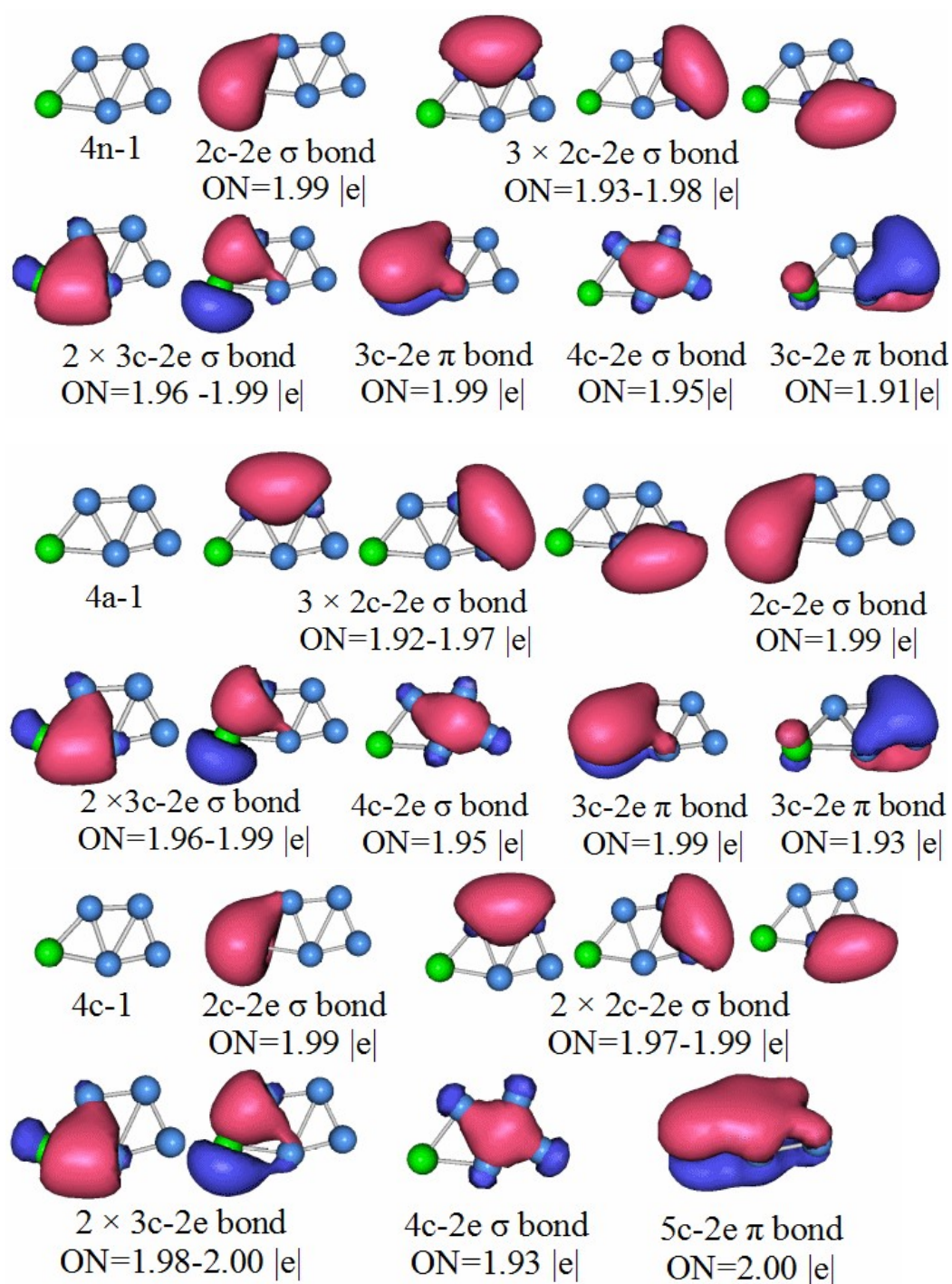


Figure 7. 4n-1, 4a-1, and 4c-1 are the most stable structures of PB_4 , PB_4^- , PB_4^+ , respectively. A detailed chemical bonding analysis is shown for each structure.

The 4a-1 structure is the most stable structure of the anionic cluster PB_4^- . This has nine chemical bonds. The analysis results are as follows: one 2c-2e σ bond with an ON = 1.99, three 2c-2e σ bonds with ON = 1.92 and 1.97, two 3c-2e π bonds have an ON value between 1.96 and 1.99. There are also two 3c-2e π bonds with ON values of 1.99 and 1.93, respectively. The last chemical bond is a 4c-2e σ bond and ON = 1.95. The bonding structure for 4a-1 is very similar to that of 4n-1, with some changes seen in the occupation numbers.

The 4c-1 structure is a stable structure of the anionic cluster PB_4^+ . This has eight chemical bonds. The analysis is as follows: one 2c-2e P-B σ bond with an ON = 1.99, three 2c-2e B-B σ bonds with ON = 1.97–1.99, and the two 3c-2e π bonds have ON = 1.98 and 2.00. A 4c-2e σ bond with an ON = 1.93. The last one is a 5c-2e π bond, with ON = 2.00. Compared with the 4n-1 structure, the 4c-1 has two fewer 3c-2e π bonds. However, one 5c-2e π bond was added.

Figure 8 shows the chemical bonding analysis for the neutral 5n-1 structure. 5n-1 is the stable structure of the neutral cluster PB_5 . This has 10 chemical bonds. The analysis results are as follows: one 2c-2e P-B σ bond with ON = 1.98, another 2c-2e P-B σ bond with ON = 1.96, and two 2c-2e B-B σ bonds, with ON values ranging from 1.96 to 1.97. A 3c-2e σ bond with ON = 1.99. A 3c-2e P-B σ bond with ON = 1.96. A 3c-2e P-B π bond with ON = 1.96. A 3c-2e B-B σ bond with ON = 1.99. A 4c-2e π bond with ON = 2.00. A 5c-2e σ bond with ON = 2.00.

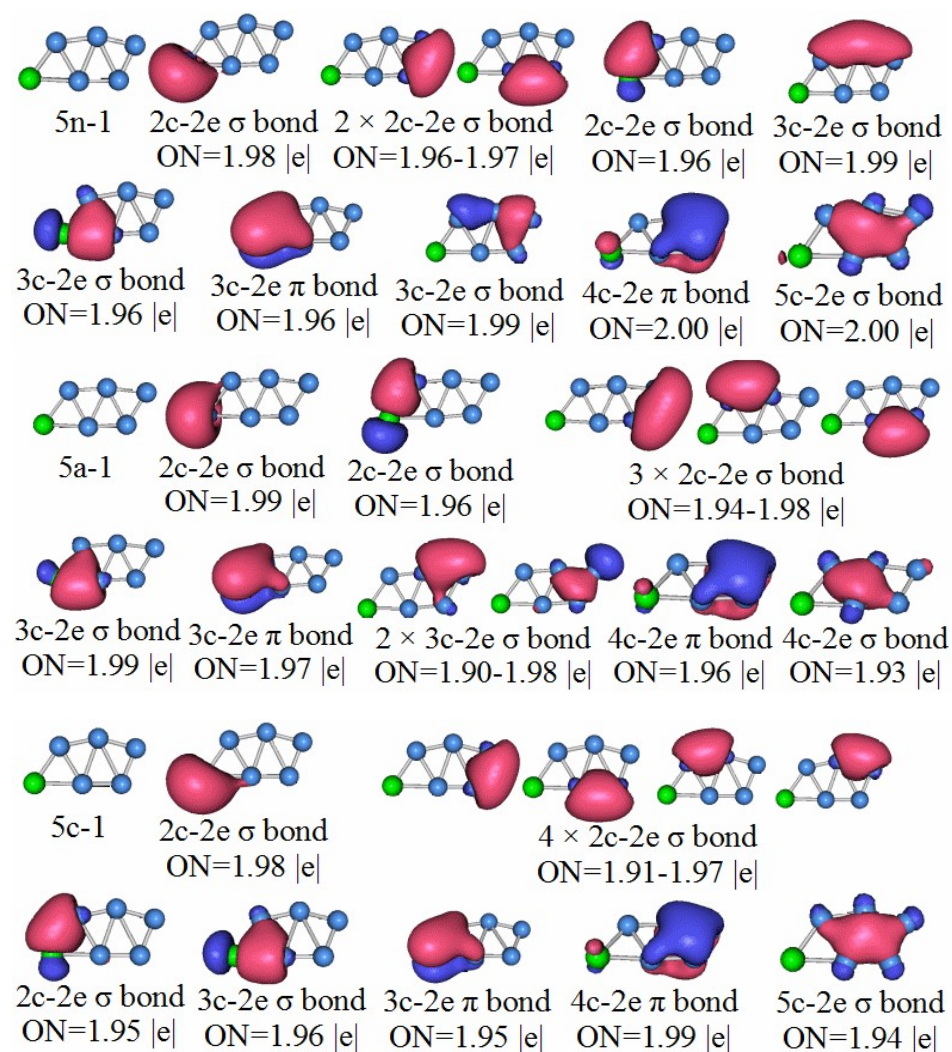


Figure 8. 5n-1, 5a-1, and 5c-1 show the most stable structures of PB_5 , PB_5^- , and PB_5^+ , respectively. A detailed chemical bonding analysis is shown.

The 5a-1 structure is the most stable structure of the PB_5^- anion cluster. This has 11 chemical bonds. The analysis results are as follows: one 2c-2e P–B σ bond with ON = 1.99; another 2c-2e P–B σ bond with ON = 1.96; the three 2c-2e σ bonds have ON values ranging from 1.94 to 1.98; a 3c-2e P–B σ bond with ON = 1.99; a 3c-2e π bond with ON = 1.97; the two 3c-2e B–B σ bonds have ON values ranging from 1.90 to 1.98; a 4c-2e π bond with ON = 1.96; a 4c-2e σ bond with ON = 1.93. Unlike 5n-1, 5a-1 has a 3c-2e B–B σ bond. In addition, the 5n-1 structure has a 5c-2e σ bond, and the 5a-1 structure has a 4c-2e σ bond.

The 5c-1 structure is the most stable structure of the cationic cluster PB_5^+ . This has 10 chemical bonds. The analysis results are as follows: the two 2c-2e P–B σ bonds have ON values of 1.98 and 1.95, respectively; the four 2c-2e B–B σ bonds have ON values ranging from 1.91 to 1.97, a 3c-2e P–B σ bond, and ON = 1.96; a 3c-2e π bond has ON = 1.95; a 4c-2e B–B π bond with ON = 1.99; the last one is a 5c-2e σ bond, with ON = 1.94. Unlike the 5n-1 structure, a 2c-2e B–B σ bond is added, and a linear 3c-2e B–B σ bond is missing.

Figure 9 shows the chemical bonding analysis for the neutral 6n-1 structure. The 6n-1 structure is the most stable structure of the neutral cluster PB_6 . This has 12 chemical bonds. The analysis results are as follows: there are two 2c-2e P–B σ bonds with ON values of 1.99 and 1.95, respectively; a 3c-2e P–B σ bond with an ON = 1.98; a 3c-2e P–B π bond with an ON = 1.92; a 4c-2e B–B π bond with an ON = 1.93; five 2c-2e B–B σ bonds, with ON values ranging from 1.91 to 1.97; finally, there are two 4c-2e B–B σ bonds, and the ON value ranges from 1.91 to 1.95.

The 6a-1 structure is the most stable structure of the anionic cluster PB_6^- . The analysis results of the 6n-1 structure are similar, and each has 12 chemical bonds. There is a small difference in partial ON values. The chemical bond analysis results are as follows: the two P–B σ bonds have ON values of 1.99 and 1.93, respectively; a 3c-2e P–B σ bond with an ON value of 1.98; a 3c-2e π bond with an ON value of 1.92; a 4c-2e B–B σ bond with an ON value of 1.93; the five 2c-2e B–B σ bonds have ON values ranging from 1.93 to 1.97; the remaining two bonds are 4c-2e σ bonds, with ON value ranging from 1.91 to 1.96.

The 6c-1 structure is the most stable structure of the cationic cluster PB_6^+ , which has 11 chemical bonds. The chemical bond analysis results are as follows: the two 2c-2e P–B σ bonds have an ON value of 1.98; the four 2c-2e B–B σ bonds have an ON value of 1.93; a 3c-2e P–B σ bond with an ON value of 1.90; the 4c-2e B–B σ bond has an ON = 1.97; a 4c-2e P–B σ bond with an ON value of 1.96; the last one is the 6c-2e B–B σ bond, whose ON value is 1.96.

Figure 10 shows the chemical bonding analysis for the neutral 7n-1 structure. The 7n-1 structure is the most stable structure of the neutral cluster PB_7 , and has a total of 13 chemical bonds. The analysis of the chemical bond results is as follows: there is a lone pair of 1c-2e bonds with an ON = 1.95; a 2c-2e B–B σ bond, with ON = 1.96; the three 2c-2e B–B σ bonds have ON values ranging from 1.94 to 1.98; the three 4c-2e B–B σ keys have ON values ranging from 1.92 to 1.96; a 3c-2e P–B π bond with an ON value of 1.98; two 3c-2e B–B σ bonds, one with an ON value of 1.98 and the other with an ON value of 1.94; the last two are the 5c-2e P–B σ bonds, and the ON values range from 1.95 to 1.96.

The 7a-1 structure is the most stable structure of the anionic cluster PB_7^- , which has 14 chemical bonds. The chemical bond analysis results are as follows: a 1c-2e lone pair has an ON value of 1.97; five 2c-2e B–B σ bonds, with ON values ranging from 1.94 to 1.98; two 2c-2e P–B σ bonds with ON values ranging from 1.96 to 1.97; a 3c-2e P–B π bond with an ON value of 1.93; two 5c-2e B–B π bonds have an ON value of 1.96; a 4c-2e B–B σ bond with an ON value of 1.98; two 5c-2e σ bonds, the ON value ranges from 1.93 to 1.94.

The 7c-1 structure is the most stable structure of the cationic cluster PB_7^+ , which has 13 chemical bonds. The chemical bond analysis results are as follows: five 2c-2e B–B σ bonds, and the ON value ranges from 1.94 to 1.97. A 1c-2e lone pair, the ON value is 1.97, the two 2c-2e P–B σ bonds, and the ON value ranges from 1.95 to 1.96. A 3c-2e P–B π bond with an ON value of 1.93. A 4c-2e B–B σ bond with an ON value of 1.97. A 5c-2e π bond with an ON value of 1.95. The two 5c-2e σ bonds, where the ON value of the P–B σ bond is 1.92, and the ON value of the P–B σ bond is 1.96.

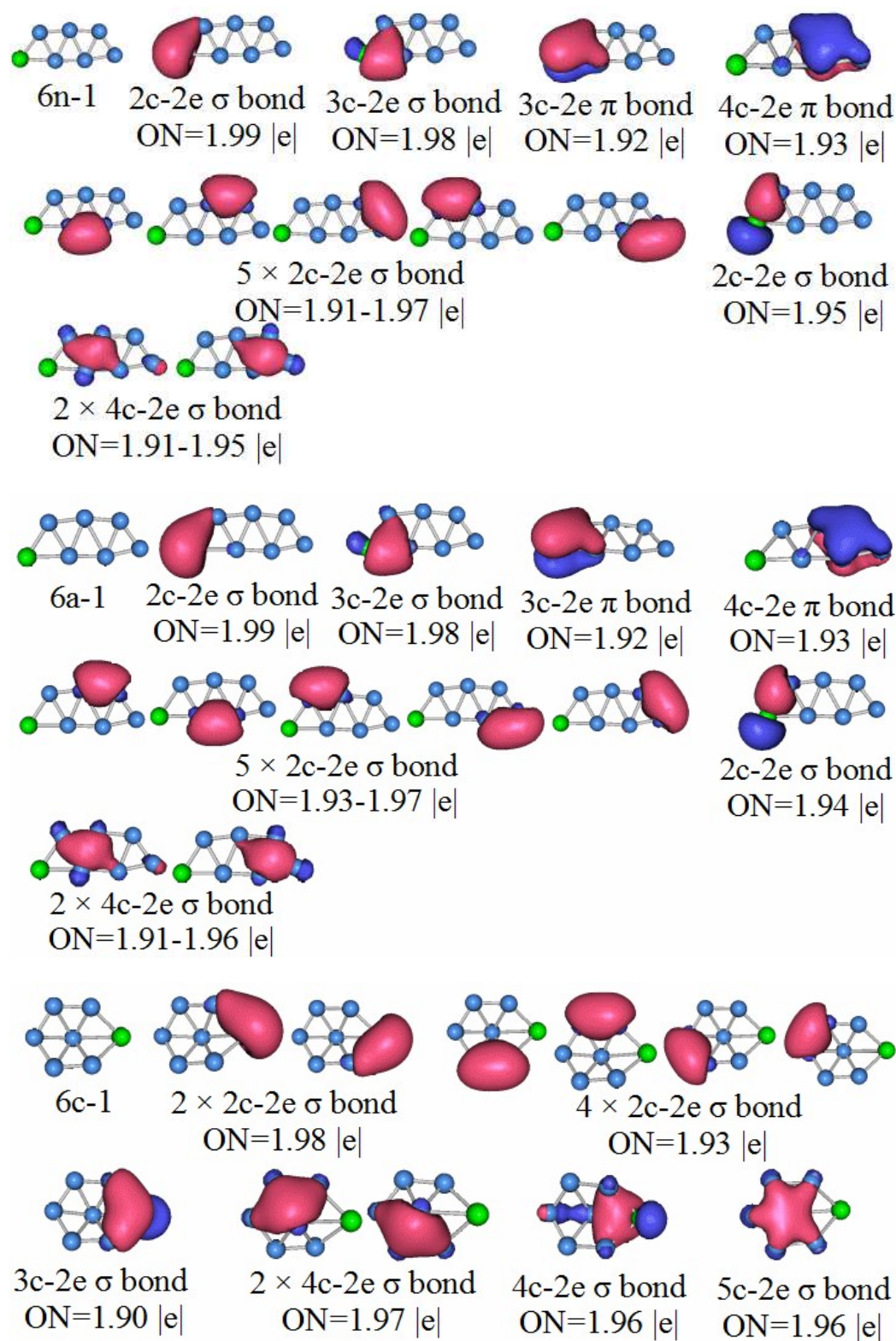


Figure 9. 6n-1, 6a-1, and 6c-1 are the most stable structures of PB_6 , PB_6^- , and PB_6^+ , respectively. Detailed chemical bonding analysis is shown.

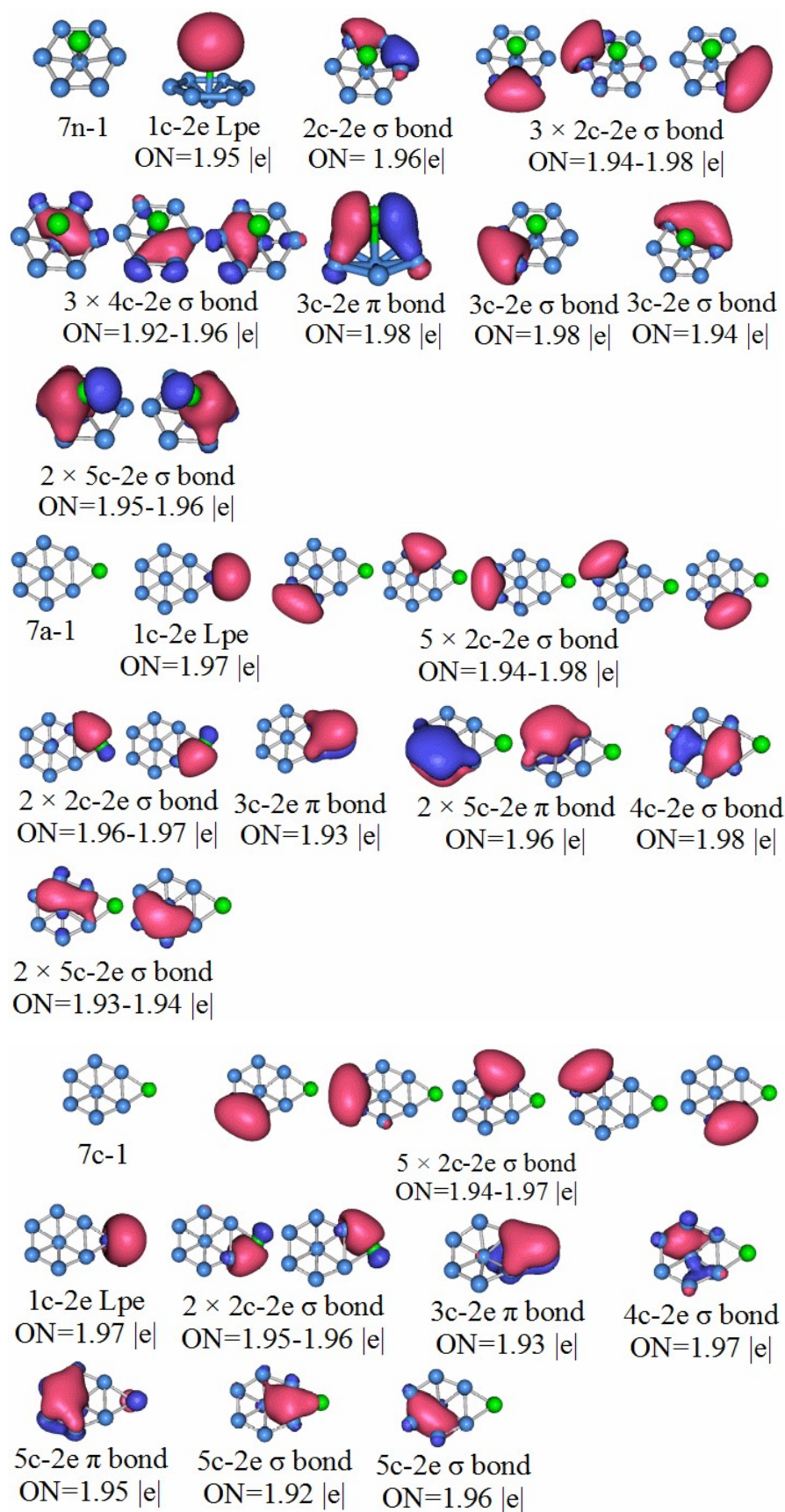


Figure 10. 7n-1, 7a-1, 7c-1 are the most stable structures of PB_7 , PB_7^- , PB_7^+ respectively. Detailed chemical bonding analysis is shown.

Figure 11 shows the chemical bonding analysis for the neutral 8n-1 structure. The 8n-1 structure is the most stable structure of the neutral cluster PB_8 , which has 15 chemical bonds. The results of the chemical bond analysis are as follows: a 1c-2e lone pair with an ON value of 1.92; two 2c-2e B-B σ bonds, with ON values ranging from 1.96 to 1.98; two 2c-2e B-B σ bonds, with ON values ranging from 1.96 to 1.97; a 4c-2e B-B σ bond with an ON value of 1.97; two linear 3c-2e B-B σ bonds with ON values ranging from 1.97 to 1.98; a 3c-2e B-B π bond with an ON value of 1.92; a 2c-2e P-B σ bond with an ON value of 1.94; a 3c-2e P-B σ bond with an ON value of 1.98; the B-B σ bond of the two 4c-2e has an ON value ranging from 1.91 to 1.95; two 5c-2e B-B π bonds with an ON value equal to 1.94.

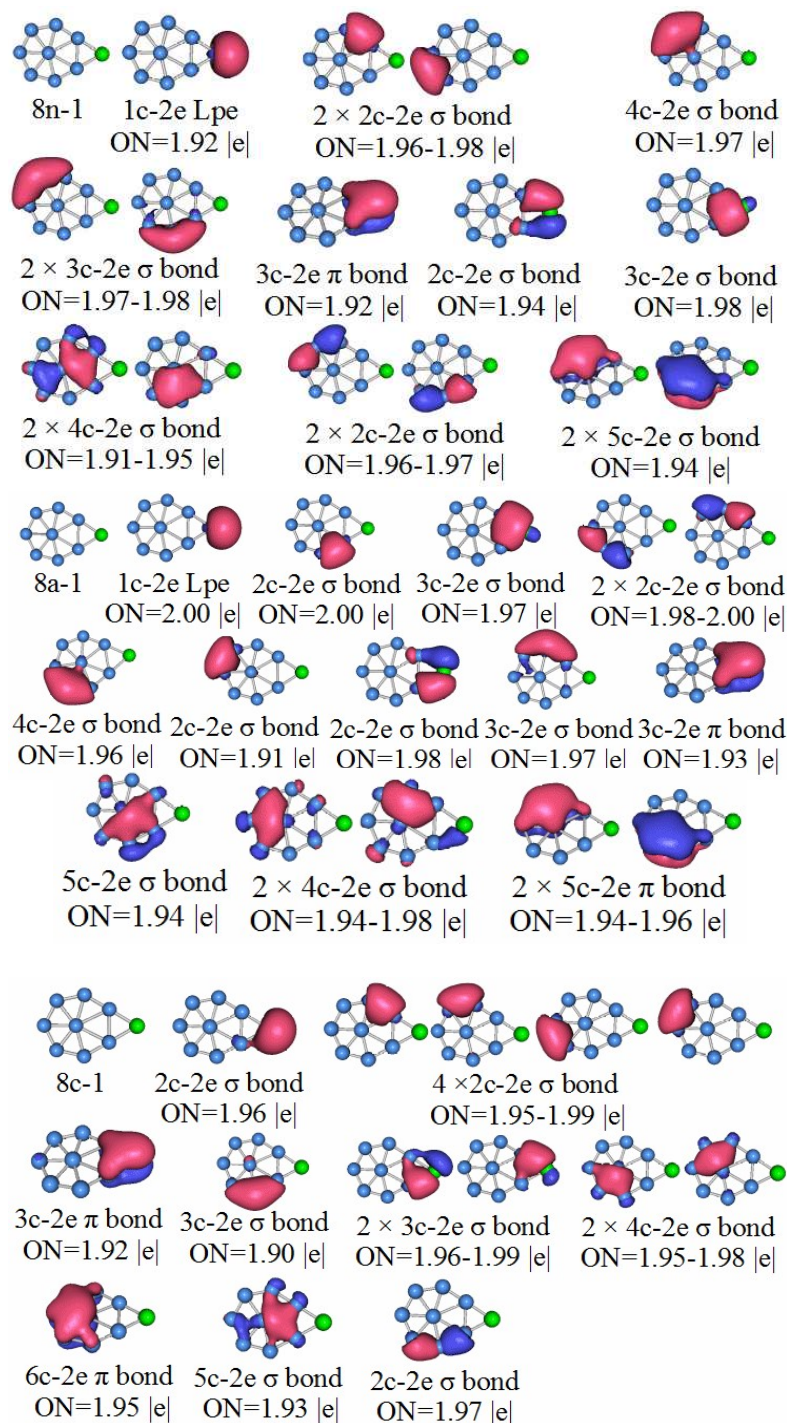


Figure 11. 8n-1, 8a-1, and 8c-1 show the most stable structures of PB_8 , PB_8^- , PB_8^+ , respectively. Detailed chemical bonding analysis is shown.

The 8a-1 structure is the most stable structure of the anionic cluster PB_8^- , which has 15 chemical bonds. The chemical bond analysis results are as follows: one 1c-2e lone electron pair, and the ON value is equal to 2.00; two 2c-2e B–B σ bonds have an ON value of 1.91 and 2.00, respectively; two special B–B σ bonds, the ON value ranges from 1.98 to 2.00; a 3c-2e P–B σ bond with an ON value of 1.97; three 4c-2e B–B σ bonds, with ON ranging from 1.94 to 1.98; a 1c-2e P–B σ bond with an ON value of 1.98; a linear σ bond of 3c-2e with an ON = 1.97; a 3c-2e P–B π bond with an ON value equal to 1.93; a 5c-2e B–B σ bond with an ON value of 1.94. The B–B π bonds of the two 5c-2e have an ON value ranging from 1.94 to 1.96.

The 8c-1 structure is the most stable structure of the cationic cluster PB_8^+ , which has 14 chemical bonds. The chemical bond analysis results are as follows: a 2c-2e P–B σ bond has an ON value of 1.96; five 2c-2e B–B σ bonds, with ON value ranging from 1.95 to 1.99; a 3c-2e P–B π bond with an ON value of 1.92; a 3c-2e B–B σ bond with an ON value equal to 1.90; the two 3c-2e P–B π bonds have ON values range from 1.96 to 1.99; two 4c-2e B–B σ bonds, the ON value ranges from 1.95 to 1.98; a 6c-2e B–B π bond with an ON value of 1.95. There is also a 5c-2e σ bond with an ON = 1.93.

Other recent work on MB_7 and MB_8 clusters ($M = Bi, La \dots$) concludes that these structures are stabilized by the double aromaticity within the B_7 and B_8 unit, which should be three delocalized sigma bonds and three delocalized pi bonds [43]. We expect that double aromaticity is also stabilizing our structures.

3.6. Infrared Spectroscopy

In order to confirm the structures of these $PB_n/PB_n^-/PB_n^+$ clusters with the experimental results, one popular method is to use infrared spectroscopy. We, therefore, calculated the infrared spectra. The simulation results are shown below and Figure 12.

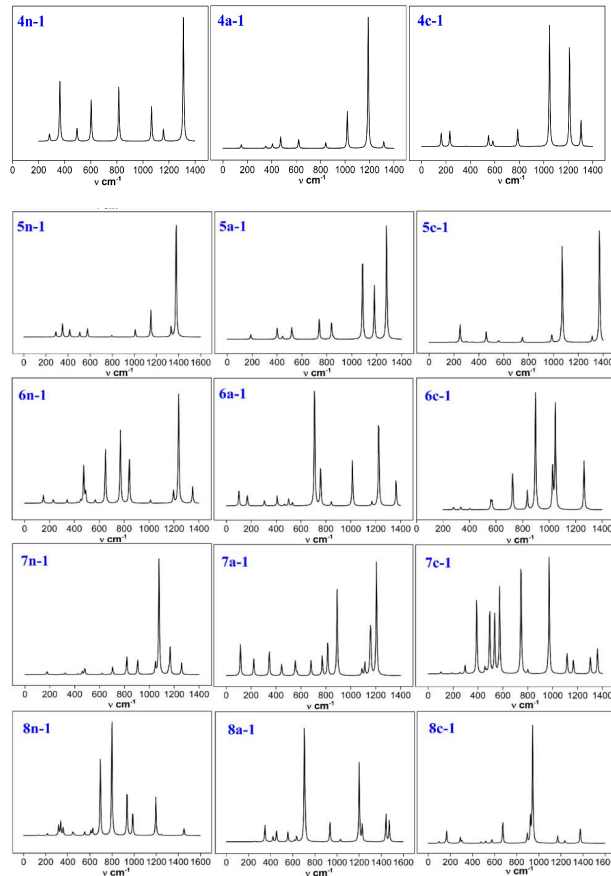


Figure 12. Calculated IR spectra of the structures of $PB_n/PB_n^-/PB_n^+$ clusters at the B3LYP/6-311+G(d) level.

3.7. Simulated Photoelectron Spectrum

Photoelectron spectroscopy uses the photoelectric effect to measure the kinetic energy of photoelectrons emitted from a sample by monochromatic radiation to determine the binding energy, the photoelectron intensity, and the angular distribution of these electrons. One can use this information to study atoms, molecules, condensed phases, and especially the electronic structure of solid surfaces. In order to predict the related properties of these materials properly, we used the TD-DFT method at the TD-B3LYP/6-311+G(d) level to calculate the VDEs. The first VDE value is the energy difference between the lowest energy structure of the anionic cluster and their neutral species at the optimized anionic geometry. Other higher VDE values are obtained by adding vertical excitation energy to the first VDE value. The results for the anion clusters PB_n^- are shown in Figure 13.

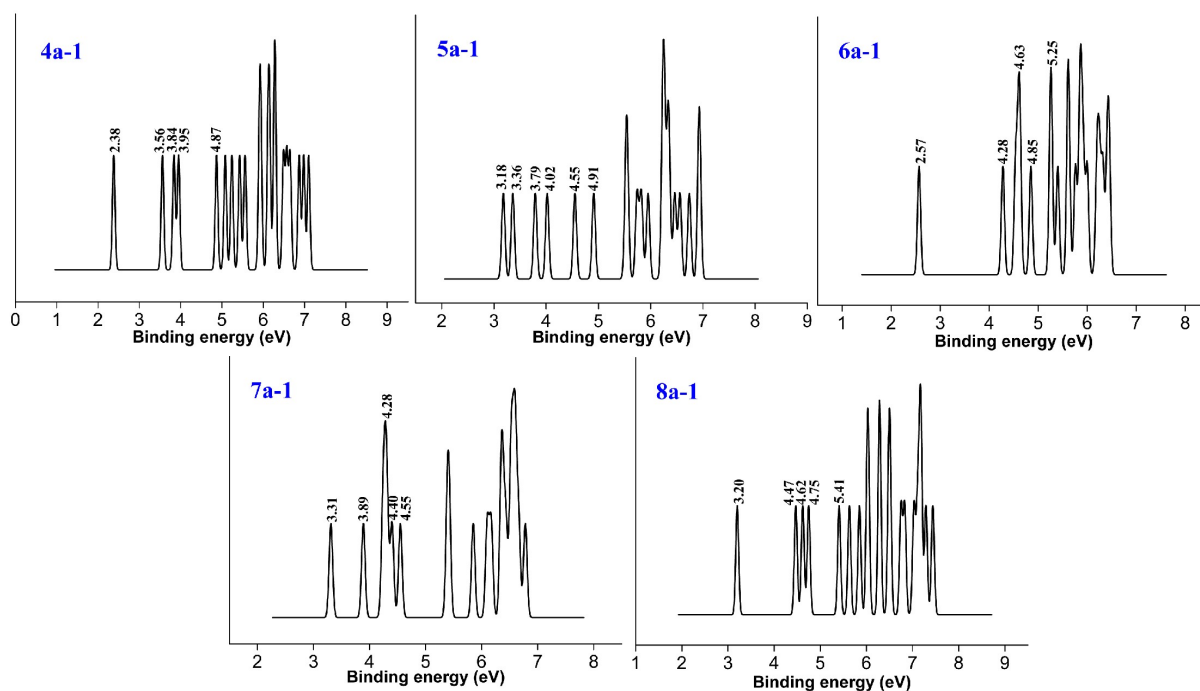


Figure 13. The simulated photoelectron spectrum for the ground-state PB_n^- anions using TD-B3LYP/6-311+G(d) with vertical detachment energies (VDE) indicated.

A PES simulation of each anion cluster is shown in Figure 13, and the energy of the ground and excited states of each structure are listed. The ground-state energies from the 4a-1 structure to the 8a-1 structure are 2.38 eV, 3.18 eV, 2.57 eV, 3.31 eV, and 3.20 eV, respectively. There are certain differences in the ground-state energy of the different structures, and there is not a linear relationship where the excited state energy gets larger as the number of atoms increases. When the difference between the first excited state energy difference and the ground-state energy is large, this indicates that the structure has strong binding to electrons. It can be seen from Figure 13 that the energy difference between the first excited state energy and the ground state of the structures 4a-1, 6a-1, and 8a-1 is greater than 1 eV, and the energy difference between the structures 5a-1 and 7a-1 is less than 1 eV. This shows that the former has a greater ability to bind electrons.

4. Conclusions

We have completed a theoretical study of the atomic clusters $PB_n/PB_n^-/PB_n^+$ ($n = 4-8$). We used density functional theory and ab initio methods to study the stability of the atomic clusters and to explore the arrangement of stable structures. Structures were searched using the Coalescence Kick method. We found that the lowest energy structures of the smaller phosphorus-doped boron clusters tend to form planar or quasi-planar structures.

As additional boron atoms are added to the smallest structures, the boron atoms expand in a zigzag arrangement or in a net-like manner, and the phosphorus atom is arranged on the periphery. For larger structures with seven or eight boron atoms, an unusual umbrella-like structure appears. We calculated the binding energy as well as different energies to study cluster stability. We calculated the ionization energy, electron affinity, and the HOMO–LUMO gaps. In addition, we used the adaptive natural density partitioning program to perform bond analysis so that we have a comprehensive understanding of the bonding. In order to have a suitable connection with the experiment, we simulated the infrared and photoelectron spectra.

Author Contributions: Conceptualization, L.-M.Y.; investigation, Q.-S.L., B.S., L.W. and L.-M.Y.; resources, E.G.; supervision, L.-M.Y.; writing—original draft, Q.-S.L., B.S., L.W. and L.-M.Y.; writing—review and editing, E.G. All authors have read and agreed to the published version of the manuscript.

Funding: Q.-S.L., B.S., L.W. and L.-M.Y. gratefully acknowledge support from the National Natural Science Foundation of China (22073033, 21873032, 21673087, 21903032), startup fund (2006013118 and 3004013105) from Huazhong University of Science and Technology, the Fundamental Research Funds for the Central Universities (2019kfyRCPY116), and the Innovation and Talent Recruitment Base of New Energy Chemistry and Device (B21003).

Institutional Review Board Statement: Not applicable.

Informed Consent Statement: Not applicable.

Data Availability Statement: Not applicable.

Acknowledgments: The work was carried out in part at the LvLiang Cloud Computing Center of China, and some of the calculations were performed on TianHe-2. The computing work in this paper is supported by the Public Service Platform of High-Performance Computing by the Network and Computing Center of HUST. The majority of the calculations were carried out at the Minnesota Supercomputing Institute. The authors acknowledge the Minnesota Supercomputer Institute for computational resources and support.

Conflicts of Interest: There are no conflict of interest to declare.

References

1. Kiran, B.; Gopa Kumar, G.; Nguyen, M.T.; Kandalam, A.K.; Jena, P. Origin of the Unusual Stability of B₁₂ and B₁₃+ Clusters. *Inorg. Chem.* **2009**, *48*, 9965. [[CrossRef](#)] [[PubMed](#)]
2. Sergeeva, A.P.; Piazza, Z.A.; Romanescu, C.; Li, W.-L.; Boldyrev, A.I.; Wang, L.-S. B₂₂[−] and B₂₃[−]: All-Boron Analogues of Anthracene and Phenanthrene. *J. Am. Chem. Soc.* **2012**, *134*, 18065. [[CrossRef](#)] [[PubMed](#)]
3. Piazza, Z.A.; Popov, I.A.; Li, W.-L.; Pal, R.; Zeng, X.C.; Boldyrev, A.I.; Wang, L.-S. A photoelectron spectroscopy and ab initio study of the structures and chemical bonding of the B₂₅− cluster. *J. Chem. Phys.* **2014**, *141*, 034303. [[CrossRef](#)] [[PubMed](#)]
4. Li, W.-L.; Pal, R.; Piazza, Z.A.; Zeng, X.C.; Wang, L.-S. B₂₇[−]: Appearance of the smallest planar boron cluster containing a hexagonal vacancy. *J. Chem. Phys.* **2015**, *142*, 204305. [[CrossRef](#)] [[PubMed](#)]
5. Li, H.R.; Jian, T.; Li, W.L.; Miao, C.Q.; Wang, Y.J.; Chen, Q.; Luo, X.M.; Wang, K.; Zhai, H.J.; Li, S.D. Competition between quasi-planar and cage-like structures in the B₂₉[−] cluster: Photoelectron spectroscopy and ab initio calculations. *Phys. Chem. Chem. Phys.* **2016**, *18*, 29147–29155. [[CrossRef](#)] [[PubMed](#)]
6. Li, W.-L.; Zhao, Y.-F.; Hu, H.-S.; Li, J.; Wang, L.-S. [B₃₀][−]: A Quasiplanar Chiral Boron Cluster. *Angew. Chem. Int. Ed.* **2014**, *53*, 5540. [[CrossRef](#)] [[PubMed](#)]
7. Li, W.-L.; Chen, Q.; Tian, W.-J.; Bai, H.; Zhao, Y.-F.; Hu, H.-S.; Li, J.; Zhai, H.-J.; Li, S.-D.; Wang, L.-S. The B₃₅ Cluster with a Double-Hexagonal Vacancy: A New and More Flexible Structural Motif for Borophene. *J. Am. Chem. Soc.* **2014**, *136*, 12257. [[CrossRef](#)]
8. Piazza, Z.A.; Hu, H.-S.; Li, W.-L.; Zhao, Y.-F.; Li, J.; Wang, L.-S. Planar hexagonal B₃₆ as a potential basis for extended single-atom layer boron sheets. *Nat. Commun.* **2014**, *5*, 3113. [[CrossRef](#)]
9. Chen, Q.; Wei, G.F.; Tian, W.J.; Bai, H.; Liu, Z.P.; Zhai, H.J.; Li, S.D. Quasi-planar aromatic B₃₆ and B₃₆− clusters: All-boron analogues of coronene. *Phys. Chem. Chem. Phys.* **2014**, *16*, 18282. [[CrossRef](#)]
10. Romanescu, C.; Harding, D.J.; Fielicke, A.; Wang, L.-S. Probing the structures of neutral boron clusters using infrared/vacuum ultraviolet two color ionization: B₁₁, B₁₆, and B₁₇. *J. Chem. Phys.* **2012**, *137*, 014317. [[CrossRef](#)]
11. Jian, T.; Chen, X.; Li, S.-D.; Boldyrev, A.I.; Li, J.; Wang, L.-S. Probing the structures and bonding of size-selected boron and doped-boron clusters. *Chem. Soc. Rev.* **2019**, *48*, 3550. [[CrossRef](#)] [[PubMed](#)]

12. Zhai, H.-J.; Kiran, B.; Li, J.; Wang, L.-S. Hydrocarbon analogues of boron clusters—Planarity, aromaticity and antiaromaticity. *Nat. Mater.* **2003**, *2*, 827. [[CrossRef](#)] [[PubMed](#)]
13. Wu, G.; Wang, J.; Zhang, X.; Zhu, L. Hydrogen Storage on Metal-Coated B80 Buckyballs with Density Functional Theory. *J. Phys. Chem. C* **2009**, *113*, 7052. [[CrossRef](#)]
14. Qi, B.; Wu, C.; Li, X.; Wang, D.; Sun, L.; Chen, B.; Liu, W.; Zhang, H.; Zhou, X. Self-Assembled Magnetic Gold Catalysts from Dual-Functional Boron Clusters. *ChemCatChem* **2015**, *10*, 2285–2290. [[CrossRef](#)]
15. Tu, D.; Cai, S.; Fernandez, C.; Ma, H.; Wang, X.; Wang, H.; Ma, C.; Yan, H.; Lu, C.; An, Z. Boron-Cluster-Enhanced Ultralong Organic Phosphorescence. *Angew. Chem. Int. Ed.* **2019**, *58*, 9129–9133. [[CrossRef](#)]
16. Warneke, J.; Hou, G.-L.; Aprà, E.; Jenne, C.; Yang, Z.; Qin, Z.; Kowalski, K.; Wang, X.-B.; Xantheas, S.S. Electronic Structure and Stability of $[B_{12}X_{12}]^{2-}$ ($X = F\text{--}At$): A Combined Photoelectron Spectroscopic and Theoretical Study. *J. Am. Chem. Soc.* **2017**, *139*, 14749–14756. [[CrossRef](#)]
17. Warneke, J.; Konieczka, S.Z.; Hou, G.-L.; Aprà, E.; Kerpen, C.; Keppner, F.; Schäfer, T.C.; Deckert, M.; Yang, Z.; Bylaska, E.J.; et al. Properties of perhalogenated $\{closo\text{-}B_{10}\}$ and $\{closo\text{-}B_{11}\}$ multiply charged anions and a critical comparison with $\{closo\text{-}B_{12}\}$ in the gas and the condensed phase. *Phys. Chem. Chem. Phys.* **2019**, *21*, 5903–5915. [[CrossRef](#)]
18. Mayer, M.; van Lessen, V.; Rohdenburg, M.; Hou, G.L.; Yang, Z.; Exner, R.M.; Apra, E.; Azov, V.A.; Grabowsky, S.; Xantheas, S.S.; et al. Rational design of an argon-binding superelectrophilic anion. *Proc. Natl. Acad. Sci. USA* **2019**, *116*, 8167–8172. [[CrossRef](#)]
19. Rohdenburg, M.; Yang, Z.; Su, P.; Bernhardt, E.; Yuan, Q.; Apra, E.; Grabowsky, S.; Laskin, J.; Jenne, C.; Wang, X.-B.; et al. Properties of gaseous $closo\text{-}[B_6X_6]^{2-}$ dianions ($X = Cl, Br, I$). *Phys. Chem. Chem. Phys.* **2020**, *22*, 17713–17724. [[CrossRef](#)]
20. Apra, E.; Warneke, J.; Xantheas, S.S.; Wang, X.B. A benchmark photoelectron spectroscopic and theoretical study of the electronic stability of $[B_{12}H_{12}]^{2-}$. *J. Chem. Phys.* **2019**, *150*, 164306. [[CrossRef](#)]
21. Czekner, J.; Cheung, L.F.; Johnson, E.L.; Fortenberry, R.C.; Wang, L.-S. A high-resolution photoelectron imaging and theoretical study of CP^- and C_2P^- . *J. Chem. Phys.* **2018**, *148*, 044301. [[CrossRef](#)] [[PubMed](#)]
22. Wen, L.; Li, Q.; Song, B.; Yang, L.; Ganz, E. The Evolution of Geometric Structures, Electronic Properties, and Chemical Bonding of Small Phosphorus-Boron Clusters. *Condens. Matter* **2022**, *7*, 36. [[CrossRef](#)]
23. Saha, P.; Rahane, A.B.; Kumar, V.; Sukumar, N. Analysis of the electron density features of small boron clusters and the effects of doping with C, P, Al, Si, and Zn: Magic B7P and B8Si clusters. *Phys. Scr.* **2016**, *91*, 053005. [[CrossRef](#)]
24. Jin, S.; Chen, B.; Kuang, X.; Lu, C.; Sun, W.; Xia, X.; Gutsev, G.L. Structural and electronic properties of medium-sized aluminum-doped boron clusters AlB_n and their anions. *J. Phys. Chem. C* **2019**, *123*, 6276–6283. [[CrossRef](#)]
25. Barroso, J.; Pan, S.; Merino, G. Structural transformations in boron clusters induced by metal doping. *Chem. Soc. Rev.* **2022**, *51*, 1098–1123. [[CrossRef](#)] [[PubMed](#)]
26. Wang, Y.J.; Guo, J.C.; Zhai, H.J. Why nanoscale tank treads move? Structures, chemical bonding, and molecular dynamics of a doped boron cluster $B_{10}C$. *Nanoscale* **2017**, *9*, 9310–9316. [[CrossRef](#)]
27. Tai, T.B.; Kadłubański, P.; Roszak, S.; Majumdar, D.; Leszczynski, J.; Nguyen, M.T. Electronic Structures and Thermochemical Properties of the Small Silicon-Doped Boron Clusters B_nSi ($n = 1\text{--}7$) and Their Anions. *ChemPhysChem* **2011**, *12*, 2948–2958. [[CrossRef](#)]
28. Gu, J.B.; Yang, X.D.; Wang, H.Q.; Li, H.F. Structural, electronic, and magnetic properties of boron cluster anions doped with aluminum: B_nAl ($2 \leq n \leq 9$). *Chin. Phys. B* **2012**, *21*, 043102. [[CrossRef](#)]
29. Anis, I.; Dar, M.S.; Rather, G.M.; Dar, M.A. Exploring the structure and electronic properties of germanium doped boron clusters using density functional theory based global optimization method. *New J. Chem.* **2022**, *46*, 6244–6254. [[CrossRef](#)]
30. Mai, D.T.T.; Duong, L.V.; Tai, T.B.; Nguyen, M.T. Electronic structure and thermochemical parameters of the silicon-doped boron clusters B_nSi , with $n = 8\text{--}14$, and their anions. *J. Phys. Chem. A* **2016**, *120*, 3623–3633. [[CrossRef](#)]
31. Chen, B.; Gutsev, G.L.; Li, D.; Ding, K. Structure and Chemical Bonding in Medium-Size Boron Clusters Doped with Praseodymium. *Inorganic Chemistry. Inorg. Chem.* **2022**, *61*, 20, 7890–7896. [[CrossRef](#)]
32. Li, D.; Gao, J.; Cheng, P.; He, J.; Yin, Y.; Hu, Y.; Chen, L.; Cheng, Y.; Zhao, J. 2D boron sheets: Structure, growth, and electronic and thermal transport properties. *Adv. Funct. Mater.* **2020**, *30*, 1904349. [[CrossRef](#)]
33. Bao, K.; Goedecker, S.; Koga, K.; Lançon, F.; Neelov, A. Structure of large gold clusters obtained by global optimization using the minima hopping method. *Phys. Rev. B* **2009**, *79*, 041405. [[CrossRef](#)]
34. Schönborn, S.E.; Goedecker, S.; Roy, S.; Oganov, A.R. The performance of minima hopping and evolutionary algorithms for cluster structure prediction. *J. Chem. Phys.* **2009**, *130*, 144108. [[CrossRef](#)] [[PubMed](#)]
35. Goedecker, S. Minima hopping: An efficient search method for the global minimum of the potential energy surface of complex molecular systems. *J. Chem. Phys.* **2004**, *120*, 9911. [[CrossRef](#)]
36. Chen, X.; Zhao, Y.-F.; Wang, L.-S.; Li, J. Recent progresses of global minimum searches of nanoclusters with a constrained Basin-Hopping algorithm in the TGMIn program. *Comput. Theor. Chem.* **2017**, *1107*, 57. [[CrossRef](#)]
37. Sergeeva, A.P.; Averkiev, B.B.; Zhai, H.-J.; Boldyrev, A.I.; Wang, L.-S. All-boron analogues of aromatic hydrocarbons: B_{17}^- and B_{18}^- . *J. Chem. Phys.* **2011**, *134*, 224304. [[CrossRef](#)]
38. Dondela, B.; Peszke, J.; Śliwa, W. Semiempirical ZINDO/S, AM1 and ab initio HF/STO-3G and HF/6-31G study of quaternary salts of diazaphenanthrenes with ethyl bromide and 1,3-dibromopropane. *J. Mol. Struct.* **2005**, *753*, 154. [[CrossRef](#)]

39. Téllez, C.A.; Hollauer, E.; Giannerini, T.; Pais da Silva, M.I.; Mondragón, M.A.; Rodríguez, J.R.; Castaño, V.M. Fourier transform infrared and Raman spectra: Semi empirical AM1 and PM3; MP2/DZV and DFT/B3LYP-6-31G (d) ab initio calculations for dimethylterephthalate (DMT). *Spectrochim. Acta Part A Mol. Biomol. Spectrosc.* **2004**, *60*, 2171. [[CrossRef](#)]
40. Oakes, R.E.; Renwick Beattie, J.; Moss, B.W.; Bell, S.E.J. Conformations, vibrational frequencies and Raman intensities of short-chain fatty acid methyl esters using DFT with 6-31G (d) and Sadlej pVTZ basis sets. *J. Mol. Struct. Theochem* **2002**, *586*, 91. [[CrossRef](#)]
41. Negishi, Y.; Kawamata, H.; Hayase, T.; Gomei, M.; Kishi, R.; Hayakawa, F.; Nakajima, A.; Kaya, K. Photoelectron spectroscopy of germanium-fluorine binary cluster anions: The HOMO-LUMO gap estimation of Gen clusters. *Chem. Phys. Lett.* **1997**, *269*, 199. [[CrossRef](#)]
42. Cehovin, A.; Mera, H.; Jensen, J.H.; Stokbro, K.; Pedersen, T.B. Role of the virtual orbitals and HOMO-LUMO gap in mean-field approximations to the conductance of molecular junctions. *Phys. Rev. B* **2008**, *77*, 195432. [[CrossRef](#)]
43. Chen, W.J.; Kulichenko, M.; Choi, H.W.; Cavanagh, J.; Yuan, D.F.; Boldyrev, A.I.; Wang, L.S. Photoelectron Spectroscopy of Size-Selected Bismuth-Boron Clusters: BiB_n-(n = 6–8). *J. Phys. Chem. A* **2021**, *125*, 6751–6760. [[CrossRef](#)] [[PubMed](#)]